Technische Universität Chemnitz
Sonderforschungsbereich 393
Numerische Simulation auf massiv parallelen Rechnern

Thomas Apel Serge Nicaise

The inf-sup condition for the Bernardi-Fortin-Raugel element on anisotropic meshes

Preprint SFB393/03-15

Abstract On a large class of two-dimensional anisotropic meshes, the inf-sup condition (stability) is proved for the triangular and quadrilateral finite element pairs suggested by Bernardi/Raugel and Fortin. As a consequence the pairs $\mathcal{P}_2 - \mathcal{P}_0$, $\mathcal{Q}_2 - \mathcal{P}_0$, and $\mathcal{Q}_2' - \mathcal{P}_0$ turn out to be stable independent of the aspect ratio of the elements.

Key Words Anisotropic mesh, inf-sup condition

AMS(MOS) subject classification 65N30

Preprint-Reihe des Chemnitzer SFB 393

SFB393/03-15 **September 2003**

Contents

1 Introduction **1**

2 Meshes **2**

3 Stability of the Bernardi-Fortin-Raugel pair **5**
3.1 Definition of the element 5
3.2 Stability for meshes from isotropic elements and boundary layer patches . . 7
3.3 Corner patches 9
3.4 Summary 12

4 Proof of (3.7) **13**
4.1 Rectangular elements 13
4.2 Triangular elements 14
4.3 Trapezoidal elements 17

5 Proof of (3.12) **19**
5.1 Rectangular elements 19
5.2 Triangular elements 19
5.3 Trapezoidal elements 21

Authors' addresses:

Thomas Apel
TU Chemnitz
Fakultät für Mathematik
D-09107 Chemnitz, Germany

apel@mathematik.tu-chemnitz.de
http://www.tu-chemnitz.de/~tap

Serge Nicaise
Université de Valenciennes et du Hainaut Cambrésis
MACS, Institut des Sciences et Techniques de Valenciennes
F–59313 - Valenciennes Cedex 9, France

snicaise@univ-valenciennes.fr
http://www.univ-valenciennes.fr/macs/nicaise

1 Introduction

Viscous flow problems can be modeled by the Navier-Stokes equations. Simpler models include the Oseen equations (a linearization of the Navier-Stokes equations) and the Stokes equations (convection is neglected). The viscosity leads in the classical formulation to a term with second order derivatives of the velocity such that the solutions of all three problems contain in general corner and edge singularities. Moreover, the convective terms in the Navier-Stokes and Oseen equations lead (in particular in the case of high Reynolds numbers) to boundary and interior layers.

Both edge singularities and layers are anisotropic phenomena, that means the solution shows little variation in one direction (e.g. along the edge and tangential to the layer) and large derivatives in the perpendicular direction. Such anisotropic phenomena can be approximated well on anisotropic meshes. Before we define them in more detail let us introduce the model problem and approximation results.

Consider the Stokes problem with Dirichlet boundary conditions in a two-dimensional domain Ω. The weak formulation is to find $u \in X = H_0^1(\Omega)^2$ and $p \in M = L_0^2(\Omega)$ such that

$$\begin{array}{lcll} a(u,v) + b(v,p) & = & (f,v) & \forall v \in X, \\ b(u,q) & = & 0 & \forall q \in M, \end{array} \tag{1.1}$$

with

$$\begin{aligned} a(u,v) &= \sum_{i=1}^{2} \int_\Omega \nabla u_i \cdot \nabla v_i, \\ b(u,q) &= -\int_\Omega q \operatorname{div} u. \end{aligned}$$

Let $\mathcal{T}_h$ be an admissible mesh of elements, and $X_h \subset X$, $M_h \subset M$, finite element spaces corresponding to $\mathcal{T}_h$. The finite element solution of (1.1) is then to find $u_h \in X_h$ and $p_h \in M_h$ such that

$$\begin{array}{lcll} a(u_h,v_h) + b(v_h,p_h) & = & (f,v_h) & \forall v_h \in X_h, \\ b(u_h,q_h) & = & 0 & \forall q_h \in M_h. \end{array} \tag{1.2}$$

For the analysis of the method we define the (mesh dependent) inf-sup constant by

$$\gamma_h := \inf_{0 \neq p_h \in M_h} \sup_{0 \neq u_h \in X_h} \frac{b(u_h,p_h)}{|u_h|_{1,\Omega} \|p_h\|_{0,\Omega}}.$$

Then the finite element error can be estimated by

$$\begin{aligned} \|u-u_h\|_{1,\Omega} &\lesssim \gamma_h^{-1} \inf_{v_h \in X_h} \|u-v_h\|_{1,\Omega} + \inf_{q_h \in M_h} \|p-q_h\|_{0,\Omega}, \\ \|p-p_h\|_{0,\Omega} &\lesssim \gamma_h^{-2} \inf_{v_h \in X_h} \|u-v_h\|_{1,\Omega} + \gamma_h^{-1} \inf_{q_h \in M_h} \|p-q_h\|_{0,\Omega}, \end{aligned} \tag{1.3}$$

see [9]. The error estimate can therefore be split into the proof of the best approximation property of the spaces and a stability property. The latter is also called inf-sup condition and requires the constant γ_h to be bounded uniformly away from zero,

$$\exists\gamma > 0 : \quad \gamma_h > \gamma \quad \forall h > 0. \tag{1.4}$$

We call meshes to be admissible when they satisfy the conditions $(\mathcal{T}_h 1)$–$(\mathcal{T}_h 5)$ in Ciarlet's standard book [10, pages 38, 51]. The ratio of the diameter of an element $T \in \mathcal{T}_h$ and the diameter of the largest ball contained in $\bar{T}$ is called aspect ratio of the element. If the aspect ratio is moderate such that the investigation of how constants in our estimates depend on it, is unnecessary, we call the elements and the meshes isotropic. If the aspect ratio becomes large we should sharpen the estimate and separate the aspect ratio from the constants. In view of (1.3) it is desirable that the uniform inf-sup constant γ from (1.4) is independent of the aspect ratio.

Several pairs of finite element spaces (X_h, M_h) satisfying condition (1.4) are known for isotropic meshes, see, e. g., [9, 12] for an overview. Results for anisotropic meshes can be found in [1, 2, 4, 6, 7, 13, 14, 15, 17]; a state of the art is given in [5].

We investigate in Section 3 a conforming low order (possibly the lowest) pair of triangular and quadrilateral finite elements, namely for the pressure piecewise constants and for the velocity piecewise (bi-)linear functions enriched with the normal components of the velocity as a degree of freedom at mid-side nodes. The elements go back to Bernardi/Raugel [8] and Fortin [11], see also [12, page 134 ff., page 153 ff.]. We will call it therefore Bernardi-Fortin-Raugel element or shortly BFR element. The main result is contained in Theorem 3.7 where we prove that condition (1.4) is satisfied for a large class of two-dimensional anisotropic meshes. As a consequence the pairs $\mathcal{P}_2 - \mathcal{P}_0$, $\mathcal{Q}_2 - \mathcal{P}_0$, and $\mathcal{Q}_2' - \mathcal{P}_0$ satisfy the same condition on the same class of meshes.

Our work is closely related to the paper [15] by Schwab, Schötzau and Stenberg. We use a similar two-level family of finite element meshes, namely a macrotriangulation combined with local refinement strategies. One difference is that we do not use hanging nodes. Another difference is that these authors use only affine quadrilateral macroelements, while we use both triangles and general regular quadrilaterals so that we have to use more general microtriangulations as well, for details see Section 2. The prize that we pay for this generality is that the velocity space on the macrotriangulation is no longer a subspace of the velocity space on the microtriangulation such that we had to introduce another projection in the stability proof to remedy this. But we believe that this leads to higher flexibility in the meshes which is closer to numerical practice.

The notation $a \lesssim b$ means the existence of a positive constant C (which is independent of $\mathcal{T}_h$) such that $a \le Cb$.

2 Meshes

To define the discretization we introduce a two-level family of meshes, that we call macro- and microtriangulation, respectively. The macrotriangulation $\mathcal{T}_H$ is a splitting of the domain Ω into triangular or quadrilateral elements Q,

$$\overline{\Omega} = \bigcup_{Q \in \mathcal{T}_H} \overline{Q},$$

which is admissible in Ciarlet's sense [10]. That means in particular that we do not admit hanging nodes. We further assume that these elements are regular (isotropic) as defined for example in [10, Section 3.1] and [12, Appendix A].

The microtriangulation $\mathcal{T}_h$ is a splitting of Ω into triangular or quadrilateral elements T,

$$\overline{\Omega} = \bigcup_{T \in \mathcal{T}_h} \overline{T},$$

which should again be admissible in Ciarlet's sense. Moreover, the restriction of the microtriangulation $\mathcal{T}_h$ to a macroelement $Q \in \mathcal{T}_H$ is assumed to be an admissible triangulation of Q. These triangulations of macroelements (patches) can be classified into several local refinement strategies. We discuss here the following ones:

Patches of isotropic elements. Q is split into isotropic elements only.

This includes simple cases with few elements only, but also situations as illustrated in Figure 2.1, right hand side.

Boundary layer patches. We admit triangular and trapezoidal elements, possibly mixed. The vertices are contained in two edges of the macroelement Q. In the case of a quadrilateral macroelement Q we assume that these two edges are opposite, see the illustration in Figure 2.2.

Note also that by construction triangles satisfy the maximal angle condition which is important for interpolation error estimates. This condition was first introduced by Synge [16, pages 209–213] and is discussed e. g. in [3, pages 44, 48f., 85].

Corner patches. We again admit either triangular or trapezoidal elements, but here we assume that two edges with a common vertex are geometrically refined, see Figure 2.3 for an illustration. We further assume that the patch can be partitioned into a finite number of patches K of isotropic elements or of boundary layer type (as described above) such that adjacent patches have the same size. These patches K need not to form an admissible mesh—we allow one hanging node per side and demand that there is an edge e of an element $T \in \mathcal{T}_h$ that joins the hanging node a of K with a node b on the opposite side of K. We assume that K is split in this way into two isotropic elements (either two quadrilaterals or a triangle and a quadrilateral). The node b belongs to the triangulation $\mathcal{T}_h$ but is not necessarily a corner of a patch K, see the partition with the thick lines in Figure 2.3.

In Subsection 3.2 we prove local stability for these strategies. Other types of refinement strategy can be included into the theory provided that local stability can be proven as well.

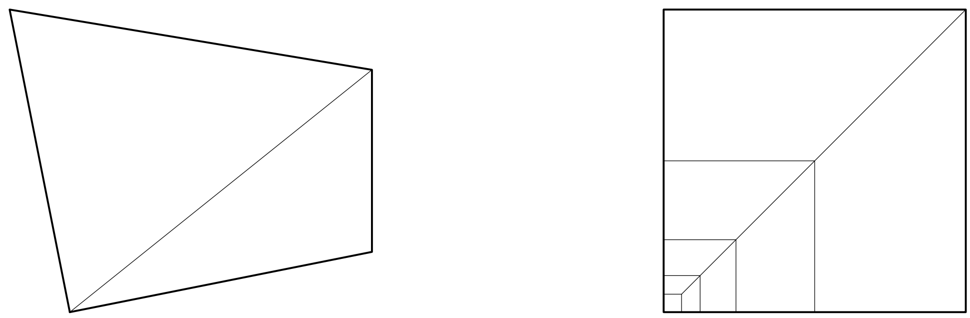

Figure 2.1: Illustration of patches with isotropic elements.

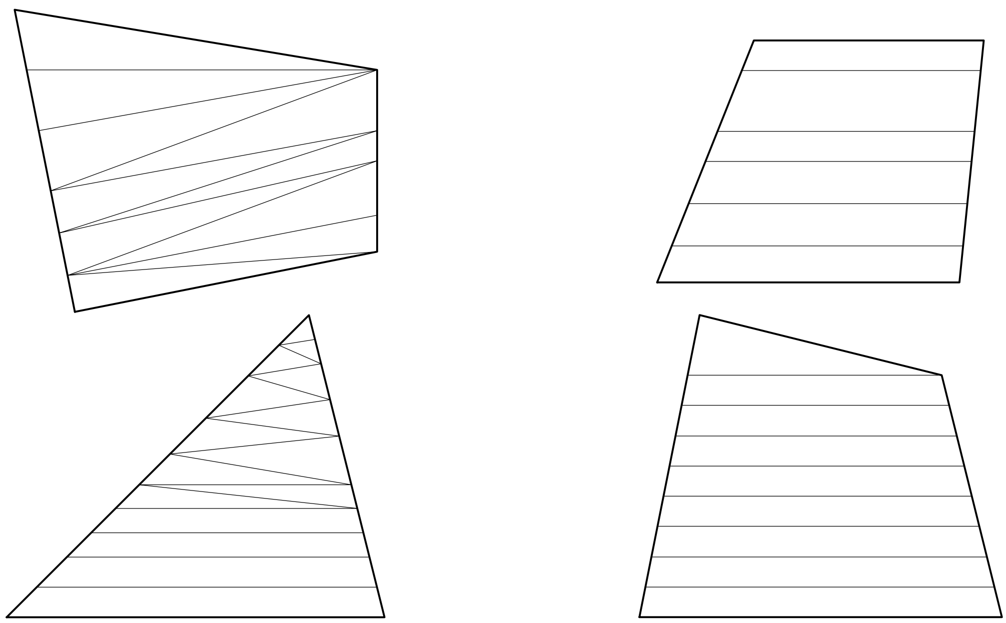

Figure 2.2: Illustration of boundary layer patches

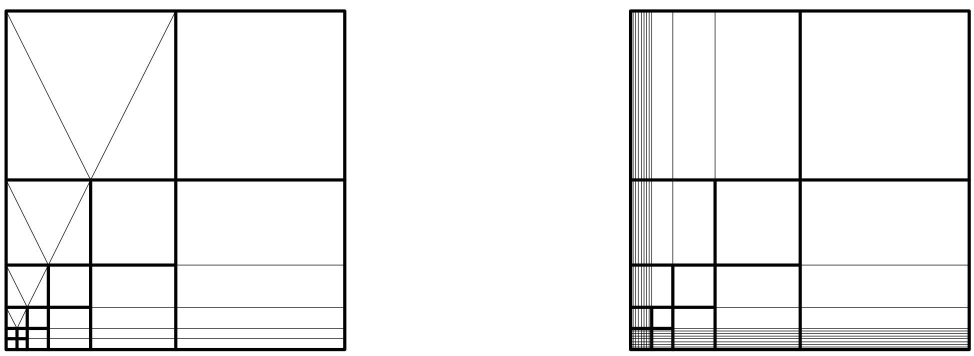

Figure 2.3: Illustration of corner patches

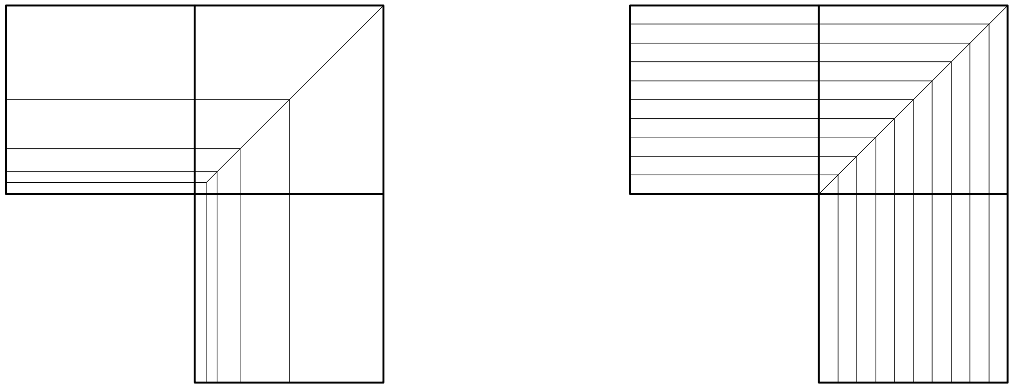

Figure 2.4: Illustration of meshes near concave corners

Figure 3.1: Illustration of the degrees of freedom for Bernardi-Fortin-Raugel elements

Remark 2.1 In order to construct a mesh in a boundary layer near a concave corner we can combine geometrically refined isotropic patches as shown in Figure 2.1 with geometrically refined boundary patches, see the illustration in Figure 2.4, left hand side. Note that the geometric refinement is necessary to ensure that the elements in the corner macro are isotropic.

Another possibility to mesh the region around a concave corner is to use only boundary layer patches, see Figure 2.4, right hand side. The mesh needs not to be equidistant like in the figure.

3 Stability of the Bernardi-Fortin-Raugel pair

3.1 Definition of the element

For the definition of the spaces we follow closely Girault/Raviart [12, page 134 ff., page 153 ff.], for an illustration see Figure 3.1. Consider first the case of triangles $T \in \mathcal{T}_h$. Denote the vertices by $a^{(i)} = (a_1^{(i)}, a_2^{(i)})^T$, $i = 1, 2, 3$, the edges by e_i, compare Figure 3.2, the corresponding outward unit normals by $n^{(i)} = (n_1^{(i)}, n_2^{(i)})^T$, and the affine nodal basis functions (barycentric coordinates) by λ_i. Then the local velocity space is defined by

$$\mathcal{P}_T := \mathcal{P}_1^2 \oplus \operatorname{span}\{n^{(1)}\lambda_2\lambda_3, n^{(2)}\lambda_3\lambda_1, n^{(3)}\lambda_1\lambda_2\}. \tag{3.1}$$

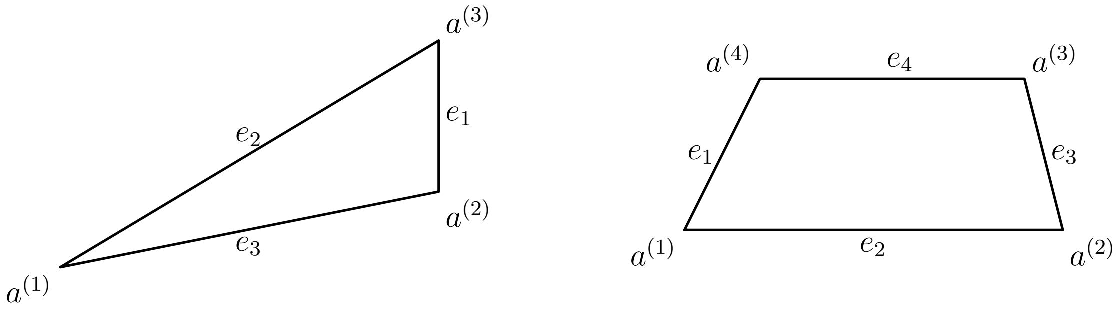

Figure 3.2: Illustration of the notation for triangles and trapezes

The local velocity space $\mathcal{P}_T$ has 9 degrees of freedom and a polynomial $v \in \mathcal{P}_T$ is uniquely defined by its values in the vertices, $v(a^{(i)})$, $i = 1, 2, 3$, and the integrals of the normal components, $\int_{e_i} v \cdot n^{(i)}$, $i = 1, 2, 3$ [12, Lemma II.2.1]. The straightforward interpolation operator $\mathrm{I}_T v$ is therefore defined by

$$\mathrm{I}_T v(a^{(i)}) = v(a^{(i)}), \quad \int_{e_i} (\mathrm{I}_T v - v) \cdot n^{(i)} = 0, \quad i = 1, 2, 3. \tag{3.2}$$

With this definition we get immediately

$$\int_T \operatorname{div}(v - \mathrm{I}_T v) = \sum_{i=1}^{3} \int_{e_i} (v - \mathrm{I}_T v) \cdot n^{(i)} = 0 \tag{3.3}$$

independent of the shape or aspect ratio of the element.

In the case that T is a quadrilateral we proceed similarly. Assume that $T = F_T(\hat{T})$ where $\hat{T} = (0,1)^2$ is the reference element and $F_T : \mathbb{R}^2 \to \mathbb{R}^2$ is a bilinear mapping. Denote the vertices of T by $a^{(i)} = (a_1^{(i)}, a_2^{(i)})^T$, $i = 1, \ldots, 4$, the edges by e_i, and the corresponding outward unit normals by $n^{(i)} = (n_1^{(i)}, n_2^{(i)})^T$. The barycentric coordinates are replaced by the reference variables $\hat{x}_1$, $\hat{x}_2$, $\hat{x}_3 = 1 - \hat{x}_1$, and $\hat{x}_4 = 1 - \hat{x}_2$. The edge bubbles on the reference element are

$$\hat{b}_1 = \hat{x}_2\hat{x}_3\hat{x}_4, \quad \hat{b}_2 = \hat{x}_1\hat{x}_3\hat{x}_4, \quad \hat{b}_3 = \hat{x}_1\hat{x}_2\hat{x}_4, \quad \hat{b}_4 = \hat{x}_1\hat{x}_2\hat{x}_3.$$

With $b_i = \hat{b}_i \circ F_T^{-1}$ we obtain the local velocity space

$$\mathcal{P}_T := \mathcal{Q}_1^2 \oplus \operatorname{span}\{n^{(i)} b_i, i = 1, \ldots, 4\}. \tag{3.4}$$

As above, a polynomial $v \in \mathcal{P}_T$ is uniquely defined by its values in the vertices and the integrals of the normal components [12, Lemma II.3.1], and the straightforward interpolation operator $\mathrm{I}_T v$ is defined by

$$\mathrm{I}_T v(a^{(i)}) = v(a^{(i)}), \quad \int_{e_i} (\mathrm{I}_T v - v) \cdot n^{(i)} = 0, \quad i = 1, \ldots, 4. \tag{3.5}$$

The global velocity space is introduced by

$$X_h := \{v \in X : v|_T \in \mathcal{P}_T \ \forall T \in \mathcal{T}_h\}. \tag{3.6}$$

Note that the restriction of an edge bubble to the edge is the same for triangles and quadrilaterals therefore the corresponding global bubble function is continuous and thus in $H^1(\Omega)$. Consequently, they are contained in X_h and not excluded by the postulation $X_h \subset X$.

Independently of X_h we will need the space X_H which is defined analogously on the macrotriangulation $\mathcal{T}_H$. Finally we introduce the spaces

$$M_h := \{q \in L_0^2(\Omega) : q|_T \in \mathcal{P}_0 \ \forall T \in \mathcal{T}_h\}, \qquad M_H := \{q \in L_0^2(\Omega) : q|_Q \in \mathcal{P}_0 \ \forall Q \in \mathcal{T}_H\}.$$

3.2 Stability for meshes from isotropic elements and boundary layer patches

We start with the proof of stability locally in the macroelements (patches). For this, define

$$\begin{aligned} X_h(Q) &:= \{v \in X_h : v = 0 \text{ in } \Omega \setminus Q\}, \\ M_h(Q) &:= \{q|_Q : q \in M_h\} \cap L_0^2(Q). \end{aligned}$$

Moreover, for any macroelement Q we define an interpolation operator $\mathrm{I}_{Q,h}$ by

$$\mathrm{I}_{Q,h} v|_T = \mathrm{I}_T v \quad \forall T \subset Q,$$

where I_T is the operator introduced in (3.2) and (3.5), respectively.

Lemma 3.1 *Let Q be a boundary layer patch. Then $\mathrm{I}_{Q,h}$ is well defined for functions $u \in H_0^1(Q)^2$ and it has the properties of a Fortin operator, namely*

$$|\mathrm{I}_{Q,h} u|_{1,Q} \lesssim |u|_{1,Q} \quad \forall u \in H_0^1(Q)^2, \tag{3.7}$$

$$\int_Q p_h \operatorname{div}(u - \mathrm{I}_{Q,h} u) = 0 \quad \forall p_h \in M_h(Q), \forall u \in H_0^1(Q)^2. \tag{3.8}$$

Proof The operator is well defined for functions from $H_0^1(Q)^2$ since all nodes lay on ∂Q where $u = 0$. Thus $\mathrm{I}_{Q,h} u$ is defined only via the edge integrals of internal edges. The stability property (3.7) is proved in Section 4. The equality (3.8) is obtained by analogy to (3.3) using that p_h is piecewise constant. □

Lemma 3.1 can now be applied to prove local stability.

Lemma 3.2 *If $Q \in \mathcal{T}_H$ is split into isotropic elements or is a boundary patch, then there exists a constant $\gamma^* > 0$ independent of both micro- and macrotriangulation, such that*

$$\sup_{v_h \in X_h(Q)} \frac{\int_Q q_h \operatorname{div} v_h}{|v_h|_{1,Q}} \geq \gamma^* \|q_h\|_{0,Q} \quad \forall q_h \in M_h(Q). \tag{3.9}$$

Proof Patches of isotropic elements are already treated in the classical literature, see for example [12, Subsections II.2.1 and II.3.1]. The idea is to construct a Fortin operator by using Clément interpolation to treat nodal values.

If Q is a boundary layer patch then the assertion is a corollary of Lemma 3.1 by using the Fortin lemma, see, for example, [12, Lemma II.1.1]. □

For the proof of global stability we shall use the macroelement technique, see, for example, [12, Theorem II.1.12]. That means we have to define a subspace $\bar{X}_h$ of X_h such that the pair $(\bar{X}_h, M_H)$ satisfies the inf-sup condition with a constant independent of H.

Since the macrotriangulation is isotropic, we know that the pair (X_H, M_H) is stable. Unfortunately, X_H is in general not a subset of X_h. The idea is to use an appropriate projection. Define the operator $\mathrm{I}_{H,h} : X_H \to X_h$ by

$$(\mathrm{I}_{H,h} v_H)|_T := \mathrm{I}_T v_H \quad \forall T \in \mathcal{T}_h. \tag{3.10}$$

Recall that the functions from X_H are continuous, even smooth in all T, such that I_T is well defined. With this projection $\mathrm{I}_{H,h}$ we define

$$\bar{X}_h := \mathrm{I}_{H,h} X_H \tag{3.11}$$

and show the inf-sup condition for the pair $(\bar{X}_h, M_H)$. We begin with the stability of $\mathrm{I}_{H,h}$.

Lemma 3.3 *The stability estimate*

$$|\mathrm{I}_T v_H|_{1,T} \lesssim |v_H|_{1,T} + H|v_H|_{2,T} \quad \forall T \subset Q \tag{3.12}$$

holds for any function $v_H \in X_H|_Q$, $Q \in \mathcal{T}_H$ arbitrary.

The proof is postponed to Section 5. Note that the difference in comparison with (3.7) is that the function v_H does in general not satisfy Dirichlet boundary conditions on ∂Q such that point values have to be used in the definition of the interpolation operator. Therefore one cannot expect to prove stability without using second order derivatives. On the other hand, the function v_H is contained in an finite dimensional space which allows to derive the following estimate (3.13) by using an inverse inequality.

Corollary 3.4 *For any function $v_H \in X_H$ the interpolation operator $\mathrm{I}_{H,h}$ has the properties of a Fortin operator, namely*

$$|\mathrm{I}_{H,h} v_H|_{1,\Omega} \lesssim |v_H|_{1,\Omega}, \tag{3.13}$$

$$\int_\Omega p_H \operatorname{div}(v_H - \mathrm{I}_{H,h} v_H) = 0 \quad \forall p_H \in M_H. \tag{3.14}$$

Proof Estimate (3.13) follows from Lemma 3.3 by using the inverse inequality on the macroelements Q,

$$|\mathrm{I}_{H,h} v_H|_{1,Q} \lesssim |v_H|_{1,Q} + H|v_H|_{2,Q} \lesssim |v_H|_{1,Q},$$

since $v_H|_Q$ is from a (maximally) 12-dimensional space and Q is isotropic and of diameter of order H. The equality (3.14) is obtained by analogy to (3.3). Note that p_H is constant in each Q. □

We are now able to prove the main result of this subsection.

Lemma 3.5 *The pair (X_h, M_h) satisfies the inf-sup condition (1.4) on meshes as described in Section 2, provided that only patches of isotropic elements and boundary layer patches are used.*

Proof As already stated above, the pair (X_H, M_H) is stable. By the Fortin lemma, see, for example, [12, Lemma II.1.1], there exists a Fortin operator $\Pi_H : X \to X_H$ with

$$|\Pi_H v|_{1,\Omega} \lesssim |v|_{1,\Omega} \quad \forall v \in X, \tag{3.15}$$

$$\int_\Omega p_H \operatorname{div}(v - \Pi_H v) = 0 \quad \forall p_H \in M_H, \forall v \in X. \tag{3.16}$$

Define now $\Pi_h = \mathrm{I}_{H,h}\Pi_H$. With (3.13) and (3.15) we obtain

$$|\Pi_h v|_{1,\Omega} = |\mathrm{I}_{H,h}\Pi_H v|_{1,\Omega} \lesssim |\Pi_H v|_{1,\Omega} \lesssim |v|_{1,\Omega} \quad \forall v \in X,$$

and with (3.14) and (3.16) we get for all $p_H \in M_H$ and for all $v \in X$

$$\begin{aligned}
\int_\Omega p_H \operatorname{div}(v - \Pi_h v) &= \int_\Omega p_H \operatorname{div}(v - \mathrm{I}_{H,h}\Pi_H v) \\
&= \int_\Omega p_H \operatorname{div}(v - \Pi_H v) + \int_\Omega p_H \operatorname{div}(\Pi_H v - \mathrm{I}_{H,h}\Pi_H v) \\
&= 0.
\end{aligned}$$

Consequently, Π_h is a Fortin operator for the pair $(\bar{X}_h, M_H)$, that means by the Fortin lemma that this pair is stable. By using the macroelement technique [12, Theorem II.1.12] we have proved the assertion. □

3.3 Corner patches

A corner patch is itself a mesh that consists of patches K of isotropic elements and boundary layer patches. If the patches form an admissible macrotriangulation, the local stability result follows from the arguments in the previous subsection.

The difficulty consists in allowing hanging nodes in this macrotriangulation. For the proof we can essentially follow [15, Section 4]. There, in Subsection 4.2, stability of the BFR element is proved in the special case where the triangulation of the macroelement is an affine image of a reference mesh. We show here that this result remains valid for the more general corner patches as introduced in Section 2.

Lemma 3.6 *For a corner patch $Q \in \mathcal{T}_H$ there exists a constant $\gamma^* > 0$ independent of both micro- and macrotriangulation, such that (3.9) holds.*

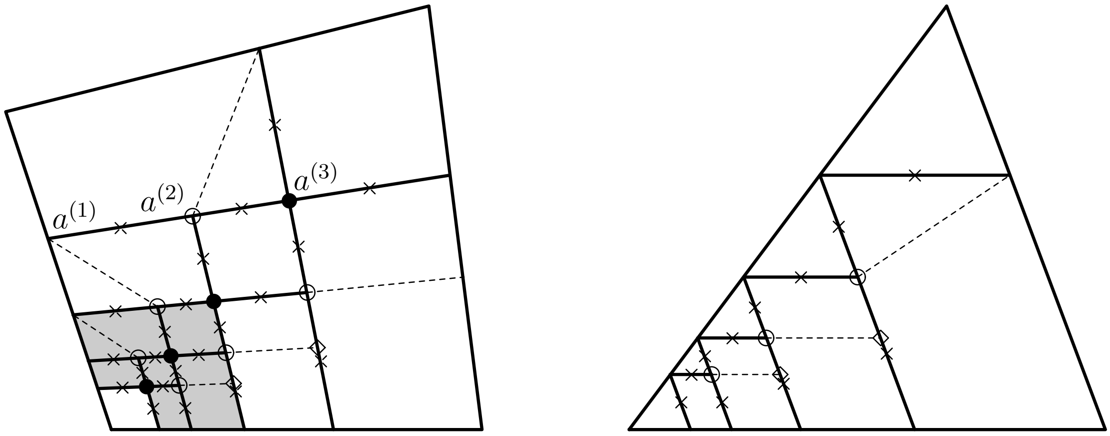

Figure 3.3: Illustration of notation in corner patches

Proof We start with the introduction of some notation. By definition a corner patch can be partitioned into a finite number of patches K, we denote this partition by $\mathcal{T}_\hbar$. All nodes of this triangulation are either *regular* (interior) *nodes*, *hanging nodes*, or *boundary nodes.* In Figure 3.3 we indicate regular nodes by a bullet and hanging nodes by a circle. All interior edges in this triangulation that do not contain a hanging node are called *regular edges.* They are marked with a cross in Figure 3.3. Note that the edges $a^{(1)}a^{(2)}$ and $a^{(2)}a^{(3)}$ are regular, but $a^{(1)}a^{(3)}$ is not.

According to the definition there is an edge for each node—we call it *irregular edge*—that joins the hanging node a of K with a node b on the opposite side of K. In this way the element is split into two subelements. Examples of irregular edges are shown in Figure 3.3 by a dashed line. Note that the set of regular and irregular edges still does not define an admissible mesh because of the nodes that are indicated by a diamond.

For each regular node $a^{(i)}$ we introduce a piecewise (bi)linear basis function φ_i with isotropic support ω_i. We assume that it is continuous and vanishes in all boundary nodes and in all other regular nodes. In hanging nodes it may have the value 0 or $\frac{1}{2}$. The support of one basis function is shaded in Figure 3.3. Furthermore, we define for each regular edge e_i an edge bubble function b_i in the same way as in Subsection 3.1. The support of such a function is isotropic and consists of two (sub)elements.

We define now a local velocity space by

$$\mathcal{P}_K := \operatorname{span}\{\varphi_i : a^{(i)} \in \bar{K} \text{ is a regular node}\}^2 \oplus \operatorname{span}\{b_i n^{(i)} : e_i \subset \bar{K} \text{ is a regular edge}\}. \tag{3.17}$$

In this definition we mean with $n^{(i)}$ the outer normal of e_i. Note that this space might be different from that defined in Subsection 3.1 since edges with hanging node induce two bubble functions. The velocity space $X_\hbar(Q) \subset H_0^1(Q)^2$ and the pressure space $M_\hbar(Q) \subset L_0^2(Q)$ over the corner patch Q are now introduced by

$$\begin{aligned} X_\hbar(Q) &:= \{v \in H_0^1(Q)^2 : v|_K \in \mathcal{P}_K \ \forall K \in \mathcal{T}_\hbar\}, \\ M_\hbar(Q) &:= \{q \in L_0^2(Q) : q|_K \in \mathcal{P}_0 \ \forall K \in \mathcal{T}_\hbar\}. \end{aligned}$$

Note that, similarly to Subsection 3.2, $X_\hbar(Q)$ is in general not a subspace of $X_h(Q)$. This deficiency is again remedied by a projection.

We are now prepared to prove the lemma. In a first step we introduce the Clément interpolant $\mathrm{C}_\hbar$ by

$$\mathrm{C}_\hbar v := \sum_i \left(|\omega_i|^{-1} \int_{\omega_i} v \right) \varphi_i$$

where the sum extends over all regular nodes. We cannot use the standard relation $\mathrm{C}_\hbar v = v$ for all $v \in \mathcal{P}_0$ here since all elements have boundary nodes or hanging nodes. But we still get

$$\sum_K \left[(\operatorname{diam} K)^{-1} \|v - \mathrm{C}_\hbar v\|_{0,K} + |v - \mathrm{C}_\hbar v|_{1,K} \right] \le |v|_{1,Q} \quad \forall v \in H_0^1(Q)$$

since the support of all basis functions contains part of the boundary ∂Q where v vanishes such that the Poincaré–Friedrichs inequality can be applied.

As in the standard proof, see [12, Subsections II.2.1 and II.3.1] we can now define the operator $\Pi_\hbar : H_0^1(Q) \to X_\hbar$

$$\begin{aligned} \Pi_\hbar v(a) &= \mathrm{C}_\hbar v(a) \quad \forall \text{ regular nodes } a, \\ \int_e (\Pi_\hbar v - v) \cdot n &= 0 \quad \forall \text{ regular edges } e, \end{aligned}$$

and prove that

$$|\Pi_\hbar v|_{1,Q} \lesssim |v|_{1,Q} \quad \forall v \in X_\hbar(Q), \tag{3.18}$$

$$\int_Q \operatorname{div}(v - \Pi_\hbar v)\, q_\hbar = 0 \quad \forall q_\hbar \in M_\hbar(Q). \tag{3.19}$$

We can now proceed as in Subsection 3.2. We define the operator $\mathrm{I}_{\hbar,h} : X_\hbar(Q) \to X_h(Q)$ by

$$(\mathrm{I}_{\hbar,h} v_\hbar)|_T := \mathrm{I}_T v_\hbar \quad \forall T \in \mathcal{T}_h,$$

the space $\bar{X}_h(Q) := \mathrm{I}_{\hbar,h} X_\hbar(Q) \subset X_h(Q)$, and the operator $\Pi_h := \mathrm{I}_{\hbar,h}\Pi_\hbar$, and we obtain the estimates

$$\begin{aligned} |\mathrm{I}_{\hbar,h} v_\hbar|_{1,\Omega} &\lesssim |v_\hbar|_{1,\Omega}, \\ \int_\Omega p_\hbar \operatorname{div}(v_\hbar - \mathrm{I}_{\hbar,h} v_\hbar) &= 0 \quad \forall p_\hbar \in M_\hbar. \end{aligned}$$

Together with (3.18) and (3.19) we derive

$$\begin{aligned} |\Pi_h v|_{1,\Omega} &\lesssim |v|_{1,\Omega} \quad \forall v \in X(Q), \\ \int_\Omega p_\hbar \operatorname{div}(v - \Pi_h v) &= 0 \quad \forall p_\hbar \in M_\hbar, \forall v \in X(Q), \end{aligned}$$

from which we conclude the local inf-sup stability. $\square$

3.4 Summary

Theorem 3.7 *The pair (X_h, M_h) satisfies the inf-sup condition (1.4) on meshes as described in Section 2.*

The proof is that of Lemma 3.5 since we did not use that the patches have a special structure. It is only necessary that a local stability result is available for all patches. We underline here that we can include further types of patches and need only to prove local stability.

Corollary 3.8 *All element pairs with the same pressure space (piecewise constants) but a larger velocity space are of course also stable, see the definition of the inf-sup constant. That means that on the meshes considered here we have proved stability for the $\mathcal{P}_2 - \mathcal{P}_0$, $\mathcal{Q}_2 - \mathcal{Q}_0$, and $\mathcal{Q}_2' - \mathcal{Q}_0$ pairs. (The space $\mathcal{Q}_2' \subset \mathcal{Q}_2$ is the 8-node quadratic serendipity element.)*

Note that the pairs $\mathcal{P}_2 - \mathcal{P}_0$ and $\mathcal{Q}_2 - \mathcal{Q}_0$ were already treated in [14, 15] but trapezoidal anisotropic meshes were not admitted there.

Remark 3.9 As introduced in Section 2 corner patches can be defined as the tensor product of one-dimensional geometric meshes, consider for example the mesh with the nodes (x_i, y_j),

$$x_0 = 0,\ x_i + 1 = \sigma^{n-i}, \qquad y_0 = 0,\ y_j = \sigma^{n-j}, \qquad i, j = 1, \ldots, n.$$

Note, however, that the inf-sup constant depends on the value of σ, $\gamma_h = \gamma_h(\sigma)$, where $\lim_{\sigma\to 0} \gamma_h(\sigma) = 0$. This can be derived from [15, Remark 3.5, page 678f.] where this statement was shown for the $\mathcal{Q}_2 - \mathcal{Q}_0$ pair. In our case the pressure space is the same but the velocity space is a subspace of $\mathcal{Q}_2$ such that the inf-sup constant can only be smaller.

On the other hand, our proof shows that the inf-sup constant in boundary layer patches does not depend on the ratio of the sizes of adjacent elements. This difference is tried to be illustrated in Figure 2.3 (right hand side) where adjacent bold rectangles are of comparable size (factor $1 \ldots 4$) whereas the elements in the boundary layer are much thinner than the first element outside this layer.

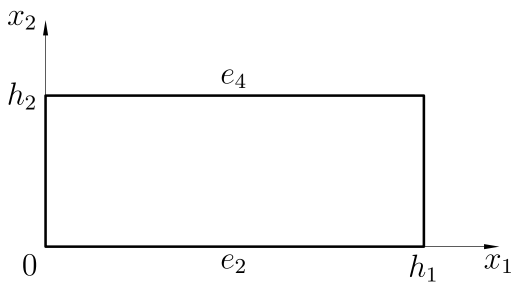

Figure 4.1: Illustration of a rectangular element T

4 Proof of (3.7)

4.1 Rectangular elements

We start with the investigation of the simplest case, namely rectangular elements, to elucidate the main ideas. We can do all considerations in a single element T. For this we introduce a coordinate system such that $T = (0, h_1) \times (0, h_2)$ and denote the long edges by e_2 and e_4, see Figure 4.1. Recall further that the element T is an element in a boundary layer patch, that means, the small edges are part of the boundary ∂Q of the macroelement. Therefore we can use that the function u to be interpolated vanishes at the small edges of T.

Denote by $b(x_1) = h_1^{-2} x_1(h_1 - x_1)$ the bubble function at the edges e_2 and e_4, and by $\varphi_1(x_2) = 1 - h_2^{-1} x_2$, $\varphi_2(x_2) = h_2^{-1} x_2$ the linear nodal hat functions. Then

$$
\begin{aligned}
\mathrm{I}_T v &= d_4\, b(x_1)\varphi_2(x_2)\begin{bmatrix} 0 \\ 1 \end{bmatrix} + d_2\, b(x_1)\varphi_1(x_2)\begin{bmatrix} 0 \\ -1 \end{bmatrix} \\
(\partial_1 \mathrm{I}_T v)_2 &= b'(x_1)(d_4\varphi_2(x_2) - d_2\varphi_1(x_2)) \\
(\partial_2 \mathrm{I}_T v)_2 &= b(x_1) h_2^{-1}(d_4 + d_2)
\end{aligned}
$$

with

$$
d_4 = \frac{\displaystyle\int_{e_4} v \cdot \begin{bmatrix} 0 \\ 1 \end{bmatrix}}{\displaystyle\int_{e_4} b(x_1)} = \frac{\displaystyle\int_{e_4} v_2}{\displaystyle\int_{e_4} b(x_1)}, \qquad d_2 = \frac{\displaystyle\int_{e_2} v \cdot \begin{bmatrix} 0 \\ -1 \end{bmatrix}}{\displaystyle\int_{e_2} b(x_1)} = -\frac{\displaystyle\int_{e_2} v_2}{\displaystyle\int_{e_2} b(x_1)}.
$$

So we can compute

$$
\begin{aligned}
\|b'(x_1)\varphi_2(x_2)\|_{0,T} &= \|b'(x_1)\varphi_1(x_2)\|_{0,T} = \tfrac{1}{3} h_1^{-1} |T|^{1/2}, \\
\|b(x_1)\|_{0,T} &= \tfrac{1}{30}\sqrt{30}\, |T|^{1/2}, \\
\|\partial_1 \mathrm{I}_T v\|_{0,T} &\le |d_4|\, \|b'(x_1)\varphi_2(x_2)\|_{0,T} + |d_2|\, \|b'(x_1)\varphi_1(x_2)\|_{0,T} \\
&\lesssim h_1^{-1}|T|^{1/2}(|d_4| + |d_2|), \qquad (4.1) \\
\|\partial_2 \mathrm{I}_T v\|_{0,T} &= \tfrac{1}{30}\sqrt{30}\, h_2^{-1}|T|^{1/2}|d_4 + d_2|. \qquad (4.2)
\end{aligned}
$$

The first expression, the left hand side of (4.1), is estimated only roughly due to the triangle inequality. The essential point is that the second expression, (4.2), must be treated carefully due to the factor h_2^{-1}.

The terms $|d_i|$, $i=2,4$, are estimated by the trace theorem and the Poincaré inequality (v is zero on the small edges) with the proper scaling introduced by the transformation $x_i = h_i \hat{x}_i$, $i=1,2$, to the reference element $\hat{T}$:

$$\begin{aligned} |d_i| &= 6h_1^{-1} \left| \int_{e_i} v_2 \right| = 6 \left| \int_{\hat{e}_i} \hat{v}_2 \right| \lesssim \int_{\hat{e}_i} |\hat{v}_2| \lesssim \|\hat{v}_2\|_{1,\hat{T}} \\ &\lesssim |\hat{v}_2|_{1,\hat{T}} \lesssim |T|^{-1/2} \sum_{i=1}^{2} h_i \|\partial_i v_2\|_{0,T} \lesssim |T|^{-1/2} h_1 |v_2|_{1,T}. \end{aligned} \tag{4.3}$$

With (4.1) we obtain

$$\|\partial_1 \mathrm{I}_T v\|_{0,T} \lesssim |v_2|_{1,T}. \tag{4.4}$$

For $|d_2 + d_4|$ we use that $v = 0$ on the small edges and the Gauß integral theorem:

$$|d_2 + d_4| = 6h_1^{-1} \left| \sum_{i=2,4} \int_{e_i} v \cdot n \right| = 6h_1^{-1} \left| \int_{\partial T} v \cdot n \right| = 6h_1^{-1} \left| \int_T \operatorname{div} v \right| \lesssim h_1^{-1} |T|^{1/2} |v|_{1,T}.$$

With (4.2) and $|T| = h_1 h_2$ we get

$$\|\partial_2 \mathrm{I}_T v\|_{0,T} \lesssim |v|_{1,T}. \tag{4.5}$$

Summation of (4.4) and (4.5) yields the desired estimate locally in each element $T \subset Q$.

Note that the x_1-derivative could equally well be estimated by using the inverse inequality,

$$\|\partial_1 \mathrm{I}_T v\|_{0,T} \lesssim h_1^{-1} \|\mathrm{I}_T v\|_{0,T} \lesssim h_1^{-1} |T|^{1/2} (|d_1| + |d_2|),$$

and (4.3).

4.2 Triangular elements

Consider now a triangular element $T \subset Q$. We locate the coordinate system such that the shortest side is parallel to the x_2-axis and the opposite vertex lays in the origin. Further notation is introduced in Figure 4.2. Note that the angles α_2 or α_3 could also be negative.

The interpolant is defined as

$$\mathrm{I}_T v = d_2 \, \lambda_1 \lambda_3 \, n^{(2)} + d_3 \, \lambda_1 \lambda_2 \, n^{(3)}$$

with

$$\begin{aligned} \lambda_1 = \lambda_1(x_1, x_2) &= 1 - h_1^{-1} x_1 \\ \lambda_2 = \lambda_2(x_1, x_2) &= (h_1 \sin(\alpha_2 - \alpha_3))^{-1} \cos\alpha_3 \, (x_1 \sin\alpha_2 - x_2 \cos\alpha_2) \\ \lambda_3 = \lambda_3(x_1, x_2) &= (h_1 \sin(\alpha_3 - \alpha_2))^{-1} \cos\alpha_2 \, (x_1 \sin\alpha_3 - x_2 \cos\alpha_3) \end{aligned}$$

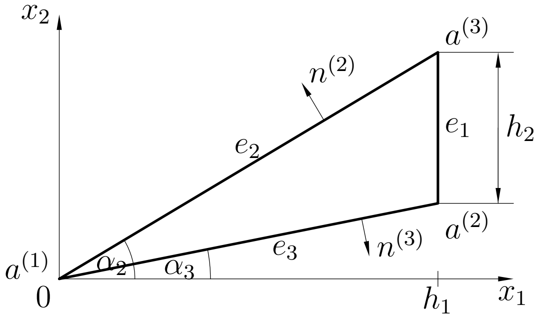

$$a^{(1)} = \begin{bmatrix} 0 \\ 0 \end{bmatrix}$$

$$a^{(2)} = h_1 \begin{bmatrix} 1 \\ \tan\alpha_3 \end{bmatrix}$$

$$a^{(3)} = h_1 \begin{bmatrix} 1 \\ \tan\alpha_2 \end{bmatrix}$$

Figure 4.2: Illustration of the notation in a triangular element T

and

$$d_2 = \frac{\int_{e_2} v \cdot n^{(2)}}{\int_{e_2} \lambda_1 \lambda_3} = (\tfrac{1}{6}|e_2|)^{-1} \int_{e_2} v \cdot n^{(2)}, \qquad d_3 = (\tfrac{1}{6}|e_3|)^{-1} \int_{e_3} v \cdot n^{(3)}.$$

We start by considering the x_2-derivative. Since λ_1 does not depend on x_2, and because $|e_2| = h_1(\cos\alpha_2)^{-1}$, $|e_3| = h_1(\cos\alpha_3)^{-1}$, we have

$$\begin{aligned}
\partial_2 \mathrm{I}_T v &= \lambda_1 [d_2 \partial_2 \lambda_3 n^{(2)} + d_3 \partial_2 \lambda_2 n^{(3)}] \\
&= 6\lambda_1 \left(|e_2|^{-1} \left(\int_{e_2} v \cdot n^{(2)} \right) (h_1 \sin(\alpha_3 - \alpha_2))^{-1} \cos\alpha_2 \, (-\cos\alpha_3) \begin{bmatrix} -\sin\alpha_2 \\ \cos\alpha_2 \end{bmatrix} + \right. \\
&\quad \left. + |e_3|^{-1} \left(\int_{e_3} v \cdot n^{(3)} \right) (h_1 \sin(\alpha_2 - \alpha_3))^{-1} \cos\alpha_3 \, (-\cos\alpha_2) \begin{bmatrix} \sin\alpha_3 \\ -\cos\alpha_3 \end{bmatrix} \right) \\
&= 6\lambda_1 (h_1 \sin(\alpha_2 - \alpha_3))^{-1} \cos\alpha_2 \cos\alpha_3 \, h_1^{-1} \, A
\end{aligned} \tag{4.6}$$

with

$$\begin{aligned}
A &= \begin{bmatrix} -\tan\alpha_2 \\ 1 \end{bmatrix} \int_{e_2} v \cdot n^{(2)} + \begin{bmatrix} -\tan\alpha_3 \\ 1 \end{bmatrix} \int_{e_3} v \cdot n^{(3)} \\
&= \begin{bmatrix} -\frac{1}{2}(\tan\alpha_2 + \tan\alpha_3) \\ 1 \end{bmatrix} \left(\int_{e_2} v \cdot n^{(2)} + \int_{e_3} v \cdot n^{(3)} \right) + \\
&\quad + \begin{bmatrix} -\frac{1}{2}(\tan\alpha_2 - \tan\alpha_3) \\ 0 \end{bmatrix} \left(\int_{e_2} v \cdot n^{(2)} - \int_{e_3} v \cdot n^{(3)} \right).
\end{aligned} \tag{4.7}$$

We treat now the factors separately. Due to the regularity of Q we have $|\alpha_2|, |\alpha_3| \le c_0 < \frac{\pi}{2}$, that means

$$\left| \begin{bmatrix} -\frac{1}{2}(\tan\alpha_2 + \tan\alpha_3) \\ 1 \end{bmatrix} \right| \lesssim 1. \tag{4.8}$$

By definition, the identity

$$\tan\alpha_2 - \tan\alpha_3 = h_1^{-1} a_2^{(3)} - h_1^{-1} a_2^{(2)} = h_1^{-1} h_2 \tag{4.9}$$

holds. Since $v = 0$ on $e_1 \subset \partial Q$ we obtain

$$\left| \int_{e_2} v \cdot n^{(2)} + \int_{e_3} v \cdot n^{(3)} \right| = \left| \int_{\partial T} v \cdot n \right| = \left| \int_T \operatorname{div} v \right| \lesssim |T|^{1/2} |v|_{1,T}. \tag{4.10}$$

In analogy to Subsection 4.1 we prove for $j = 2, 3$, using the trace theorem and the Poincaré inequality,

$$\begin{aligned} \left| \int_{e_j} v \cdot n^{(j)} \right| &\leq \int_{e_j} |v_1| + |v_2| \lesssim |e_j| \, |T|^{-1/2} \sum_{i=1}^{2} (h_1 \|\partial_1 v_i\|_{0,T} + h_2 \|\partial_2 v_i\|_{0,T}) \\ &\lesssim h_1^2 |T|^{-1/2} |v|_{1,T} \end{aligned} \tag{4.11}$$

Here we have used a transformation

$$\begin{bmatrix} x_1 \\ x_2 \end{bmatrix} = F(\hat{x}_1, \hat{x}_2) = \begin{bmatrix} h_1 & 0 \\ a_2^{(2)} & h_2 \end{bmatrix} \begin{bmatrix} \hat{x}_1 \\ \hat{x}_2 \end{bmatrix} + \begin{bmatrix} 0 \\ a_2^{(2)} \end{bmatrix}$$

to the reference element $\hat{T}$ with vertices in $(0,0)$, $(1,0)$ and $(0,1)$. It transforms derivatives as

$$\begin{aligned} \hat{\partial}_1 &= h_1 \partial_1, & \partial_1 &= h_1^{-1} \hat{\partial}_1, \\ \hat{\partial}_2 &= a_2^{(2)} \partial_1 + h_2 \partial_2, & \partial_2 &= h_2^{-1}(-a_2^{(2)} h_1^{-1} \hat{\partial}_1 + \hat{\partial}_2). \end{aligned}$$

Note further that $|a_2^{(2)}| \lesssim h_1$ since $T \subset Q$ and Q is a regular quadrilateral.

With (4.8)–(4.11) we can derive from (4.7) the estimate

$$|A| \lesssim |T|^{1/2} |v|_{1,T} + h_1^{-1} h_2 \, h_1^2 |T|^{-1/2} |v|_{1,T} \sim |T|^{1/2} |v|_{1,T}$$

which leads with (4.6) and

$$\sin(\alpha_2 - \alpha_3) = \cos\alpha_2 \cos\alpha_3 (\tan\alpha_2 - \tan\alpha_3) = h_1^{-1} h_2 \cos\alpha_2 \cos\alpha_3,$$

see (4.9), to

$$\begin{aligned} \|\partial_2 \mathrm{I}_T v\|_{0,T} &\lesssim \|\lambda_1\|_{0,T} |h_1 \sin(\alpha_2 - \alpha_3)|^{-1} \cos\alpha_2 \cos\alpha_3 h_1^{-1} |T|^{1/2} |v|_{1,T} \\ &\lesssim |T|^{1/2} h_2^{-1} h_1^{-1} |T|^{1/2} |v|_{1,T} \\ &\sim |v|_{1,T}. \end{aligned} \tag{4.12}$$

The estimate for the x_1-derivative is less difficult. By using the inverse inequality, the definitions of $\mathrm{I}_T v$, d_2, and d_3, and the estimate (4.11), we get

$$\begin{aligned} \|\partial_1 \mathrm{I}_T v\|_{0,T} &\lesssim h_1^{-1} \|I_T v\|_{0,T} \lesssim h_1^{-1} |T|^{1/2} (|d_2| + |d_3|) \\ &\lesssim h_1^{-1} |T|^{1/2} h_1^{-1} \left(\left| \int_{e_2} v \cdot n^{(2)} \right| + \left| \int_{e_3} v \cdot n^{(3)} \right| \right) \\ &\lesssim |v|_{1,T}. \end{aligned}$$

Thus the stability property (3.7) of I_T is also proved for triangular elements.

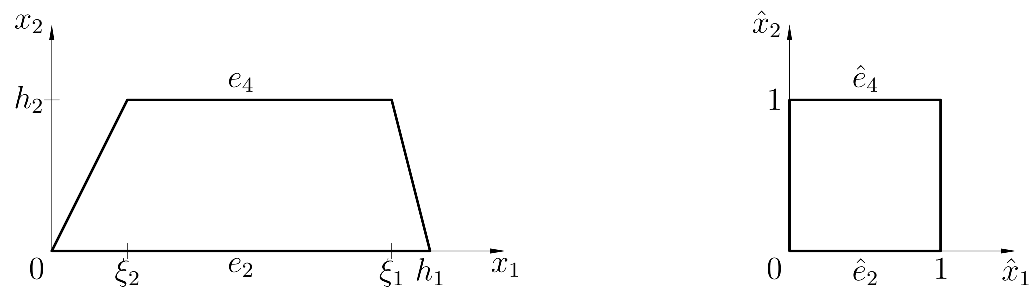

Figure 4.3: Illustration of a trapezoidal element T and the reference element $\hat{T}$

4.3 Trapezoidal elements

Trapezoidal elements can be treated by analogy to rectangular elements. One has only to be careful with the definition of the local basis functions. Since they are the image under transformation of bilinear functions in the reference element it makes sense to investigate this transformation. Introduce notation as illustrated in Figure 4.3 where we assume that

$$|\xi_2| \lesssim h_2, \qquad |h_1 - \xi_1| \lesssim h_2. \tag{4.13}$$

One can compute the transformation as

$$\begin{bmatrix} x_1 \\ x_2 \end{bmatrix} = \begin{bmatrix} h_1 \\ 0 \end{bmatrix} \hat{x}_1 + \begin{bmatrix} \xi_2 \\ h_2 \end{bmatrix} \hat{x}_2 + \begin{bmatrix} \xi_1 - h_1 - \xi_2 \\ 0 \end{bmatrix} \hat{x}_1 \hat{x}_2$$

with the Jacobian

$$\begin{aligned} J = \frac{\partial(x_1,x_2)}{\partial(\hat{x}_1,\hat{x}_2)} &= \begin{vmatrix} h_1 + (\xi_1 - h_1 - \xi_2)\hat{x}_2 & \xi_2 + (\xi_1 - h_1 - \xi_2)\hat{x}_1 \\ 0 & h_2 \end{vmatrix} \\ &= h_2(h_1 + (\xi_1 - h_1 - \xi_2)\hat{x}_2) \sim h_1 h_2 \end{aligned}$$

due to (4.13). Consequently

$$\begin{array}{ll} |\partial_1 \hat{x}_1| = J^{-1} |\hat{\partial}_2 x_2| \sim h_1^{-1}, & |\partial_2 \hat{x}_1| = J^{-1} |\hat{\partial}_2 x_1| \lesssim h_1^{-1}, \\ |\partial_1 \hat{x}_2| = J^{-1} |\hat{\partial}_1 x_2| = 0, & |\partial_2 \hat{x}_2| = J^{-1} |\hat{\partial}_1 x_1| \lesssim h_2^{-1}. \end{array} \tag{4.14}$$

As in Subsection 4.1 we have

$$\mathrm{I}_T v = d_4 b_4(x_1,x_2) \begin{bmatrix} 0 \\ 1 \end{bmatrix} + d_2 b_2(x_1,x_2) \begin{bmatrix} 0 \\ -1 \end{bmatrix}$$

where the edge bubble functions do not have the tensor product structure any more and where the d_i, $i = 2, 4$, are

$$d_i = \frac{\displaystyle\int_{e_i} v \cdot n^{(i)}}{\displaystyle\int_{e_i} b_i}. \tag{4.15}$$

For the convenience of notation we introduce w as the second component of $\mathrm{I}_T v$, $\mathrm{I}_T v = \begin{bmatrix} 0 \\ w \end{bmatrix}$. Viewing w in the reference coordinates, we get

$$\hat{w} = d_4 \hat{b}_4(\hat{x}_1, \hat{x}_2) - d_2 \hat{b}_2(\hat{x}_1, \hat{x}_2) \tag{4.16}$$

with $\hat{b}_2(\hat{x}_1, \hat{x}_2) = (1 - \hat{x}_2)\hat{x}_1(1 - \hat{x}_1)$, $\hat{b}_4(\hat{x}_1, \hat{x}_2) = \hat{x}_2\hat{x}_1(1 - \hat{x}_1)$. Moreover, we have with (4.14)

$$\begin{aligned} |\partial_1 w| &= |\hat{\partial}_1 \hat{w} \partial_1 \hat{x}_1 + \hat{\partial}_2 \hat{w} \partial_1 \hat{x}_2| \sim h_1^{-1} |\hat{\partial}_1 \hat{w}|, \\ |\partial_2 w| &= |\hat{\partial}_1 \hat{w} \partial_2 \hat{x}_1 + \hat{\partial}_2 \hat{w} \partial_2 \hat{x}_2| \lesssim h_1^{-1} |\hat{\partial}_1 \hat{w}| + h_2^{-1} |\hat{\partial}_2 \hat{w}|, \\ |w|_{1,T} &\lesssim |T|^{1/2} \left(\int_{\hat{T}} \left(h_1^{-2} |\hat{\partial}_1 \hat{w}|^2 + h_2^{-2} |\hat{\partial}_2 \hat{w}|^2 \right) \right)^{1/2} \\ &\lesssim |T|^{1/2} h_1^{-1} \left(\int_{\hat{T}} |\hat{\partial}_1 \hat{w}|^2 \right)^{1/2} + |T|^{1/2} h_2^{-1} \left(\int_{\hat{T}} |\hat{\partial}_2 \hat{w}|^2 \right)^{1/2}. \end{aligned}$$

From (4.16) we get

$$\begin{aligned} \hat{\partial}_1 \hat{w} &= \hat{x}_2(1 - 2\hat{x}_1) d_4 - (1 - \hat{x}_2)(1 - 2\hat{x}_1) d_2, \\ \hat{\partial}_2 \hat{w} &= \hat{x}_1(1 - \hat{x}_1)(d_2 + d_4), \end{aligned}$$

and consequently

$$|w|_{1,T} \lesssim |T|^{1/2} h_1^{-1} (|d_2| + |d_4|) + |T|^{1/2} h_2^{-1} |d_2 + d_4|. \tag{4.17}$$

The terms $|d_2|$ and $|d_4|$ can be estimated similarly to those in Subsection 4.1:

$$\begin{aligned} |d_j| &\sim h_1^{-1} \left| \int_{e_j} v_2 \right| \sim \left| \int_{\hat{e}_j} \hat{v}_2 \right| \le \int_{\hat{e}_j} |\hat{v}_2| \lesssim \|\hat{v}_2\|_{1,\hat{T}} \\ &\lesssim |\hat{v}_2|_{1,\hat{T}} \lesssim |T|^{-1/2} \sum_{i=1}^{2} h_i \|\partial_i v_2\|_{0,T} \lesssim |T|^{-1/2} h_1 |v_2|_{1,T}, \end{aligned} \tag{4.18}$$

$j = 2, 4$. For $|d_2 + d_4|$ we proceed slightly differently and exploit that $\int_{\hat{e}_2} \hat{b}_2 = \int_{\hat{e}_4} \hat{b}_4$:

$$\begin{aligned} |d_2 + d_4| &= \left| \frac{\int_{e_4} v_2}{\int_{e_4} b_4} - \frac{\int_{e_2} v_2}{\int_{e_2} b_2} \right| = \left| \frac{\int_{\hat{e}_4} \hat{v}_2}{\int_{\hat{e}_4} \hat{b}_4} - \frac{\int_{\hat{e}_2} \hat{v}_2}{\int_{\hat{e}_2} \hat{b}_2} \right| \sim \left| \int_{\hat{e}_4} \hat{v}_2 - \int_{\hat{e}_2} \hat{v}_2 \right| = \left| \int_{\hat{T}} \hat{\partial}_2 \hat{v}_2 \right| \\ &= |T|^{-1} \left| \int_T (\partial_1 v_2 \hat{\partial}_2 x_1 + \partial_2 v_2 \hat{\partial}_2 x_2) \right| \lesssim |T|^{-1} h_2 \int_T (|\partial_1 v_2| + |\partial_2 v_2|) \\ &\lesssim |T|^{-1} h_2 \, |T|^{1/2} |v_2|_{1,T}. \end{aligned} \tag{4.19}$$

With (4.17)–(4.19) we get the desired estimate

$$|\mathrm{I}_T v|_{1,T} = |w|_{1,T} \lesssim |v_2|_{1,T} \le |v|_{1,T}.$$

5 Proof of (3.12)

The difference in the assumptions for (3.7) and (3.12) is that the function in (3.7) satisfies Dirichlet boundary conditions on the small edges of the elements $T \subset Q$. Without having this we prove first the weaker estimate (3.12) and get the desired result (3.13) by exploiting that the function v_H is from a finite-dimensional space only.

5.1 Rectangular elements

There is nothing to prove since $X_H|_Q \subset X_h|_Q$ and therefore $\mathrm{I}_T v_H = v_H$ in T.

5.2 Triangular elements

We split the interpolant I_T into two parts,

$$\mathrm{I}_T u = \mathrm{N}_T u + (\mathrm{I}_T u - \mathrm{N}_T u). \tag{5.1}$$

The first part is the standard nodal interpolant N_T with respect to the vertices of T, and is easy to estimate using the interpolation results on anisotropic meshes [3]:

$$|\mathrm{N}_T u|_{1,T} \le |u|_{1,T} + |u - \mathrm{N}_T u|_{1,T} \lesssim |u|_{1,T} + h_1 |u|_{2,T}. \tag{5.2}$$

Using the notation of Section 4.2, the second part can be represented by

$$\mathrm{I}_T u - \mathrm{N}_T u = d_1\, \lambda_2 \lambda_3\, n^{(1)} + d_2\, \lambda_3 \lambda_1\, n^{(2)} + d_3\, \lambda_1 \lambda_2\, n^{(3)}, \tag{5.3}$$

where the coefficients d_j, $j = 1, 2, 3$, are determined to satisfy the second condition in (3.5), i.e.

$$d_j = 6|e_j|^{-1} \int_{e_j} (u - \mathrm{N}_T u) \cdot n^{(j)}. \tag{5.4}$$

We introduce the abbreviating vector function $v := u - \mathrm{N}_T u$ and note that it vanishes at the vertices of T. Let us estimate the first term on the right hand side of (5.3) by exploiting this property:

$$\begin{aligned}
\left| \int_{e_1} v \cdot n^{(1)} \right| &= \left| \int_{e_1} v_1 \right| = \left| \int_{a_2^{(2)}}^{a_2^{(3)}} (v_1(h_1, x_2) - v_1(h_1, a_2^{(2)})) \mathrm{d}x_2 \right| \\
&= \left| \int_{a_2^{(2)}}^{a_2^{(3)}} \left(\int_{a_2^{(2)}}^{x_2} \partial_2 v_1(h_1, \xi) \mathrm{d}\xi \right) \mathrm{d}x_2 \right| \\
&\le \int_{a_2^{(2)}}^{a_2^{(3)}} \int_{a_2^{(2)}}^{a_2^{(3)}} |\partial_2 v_1(h_1, \xi)| \mathrm{d}\xi \mathrm{d}x_2 = |e_1| \int_{e_1} |\partial_2 v_1| \le |e_1|^{3/2} \|\partial_2 v_1\|_{0,e_1}.
\end{aligned} \tag{5.5}$$

Recall now that v is an interpolation error and $\partial_2 = t^{(1)} \cdot \nabla$ is the derivative in (tangential) direction $t^{(1)}$ of the edge e_1. So we can use the one-dimensional interpolation error estimate

$$\|t^{(j)} \cdot \nabla (w - \mathrm{N}_T w)\|_{0,e_j} \lesssim \|t^{(j)} \cdot \nabla w\|_{0,e_j} \qquad \forall w \in H^1(e_j). \tag{5.6}$$

The properly scaled trace theorem reads

$$\|w\|_{0,e_j} \sim |e_j|^{1/2}\|\hat{w}\|_{0,\hat{e}_j} \lesssim |e_j|^{1/2}\|\hat{w}\|_{1,\hat{T}} \lesssim |e_j|^{1/2}|T|^{-1/2}(\|w\|_{0,T} + h_1|w|_{1,T}). \tag{5.7}$$

With (5.4)–(5.7) and $|e_1| = h_2$ we get

$$|d_1| \sim h_2^{-1}\left|\int_{e_1} v\cdot n^{(1)}\right| \lesssim h_2^{1/2}\|\partial_2 u_1\|_{0,e_1} \lesssim h_2|T|^{-1/2}(\|\partial_2 u_1\|_{0,T} + h_1|\partial_2 u_1|_{1,T}). \tag{5.8}$$

The desired result for the first term on the right hand side of (5.3) is now obtained by the inverse inequality:

$$\begin{aligned} |d_1\,\lambda_2\lambda_3\,n^{(1)}|_{1,T} &\lesssim |d_1|h_2^{-1}\|\lambda_2\lambda_3\|_{0,T} \\ &\lesssim h_2|T|^{-1/2}(\|\partial_2 u_1\|_{0,T} + h_1|\partial_2 u_1|_{1,T})\; h_2^{-1}|T|^{1/2} \\ &= \|\partial_2 u_1\|_{0,T} + h_1|\partial_2 u_1|_{1,T}. \end{aligned} \tag{5.9}$$

The remaining terms on the right hand side of (5.3) are treated as in Subsection 4.2. We get in analogy to (4.6) and (4.7)

$$\begin{aligned} &\partial_2(d_2\,\lambda_3\lambda_1\,n^{(2)} + d_3\,\lambda_1\lambda_2\,n^{(3)}) \\ &\quad = 6\lambda_1(h_1\sin(\alpha_2-\alpha_3))^{-1}\cos\alpha_2\cos\alpha_3\;h_1^{-1}\;A, \\ A &= \begin{bmatrix} -\frac{1}{2}(\tan\alpha_2+\tan\alpha_3) \\ 1 \end{bmatrix}\left(\int_{e_2} v\cdot n^{(2)} + \int_{e_3} v\cdot n^{(3)}\right) + \\ &\quad + \begin{bmatrix} -\frac{1}{2}(\tan\alpha_2-\tan\alpha_3) \\ 0 \end{bmatrix}\left(\int_{e_2} v\cdot n^{(2)} - \int_{e_3} v\cdot n^{(3)}\right). \end{aligned}$$

Two of the factors can be estimated as in Subsection 4.2, namely (4.8) and (4.9) are still valid. The estimate (4.10) is modified slightly where we use (5.8) and $h_2 \lesssim h_1$:

$$\begin{aligned} \left|\int_{e_2} v\cdot n^{(2)} + \int_{e_3} v\cdot n^{(3)}\right| &= \left|\int_{\partial T} v\cdot n - \int_{e_1} v\cdot n^{(1)}\right| \\ &\le \left|\int_T \operatorname{div} v\right| + \left|\int_{e_1} v\cdot n^{(1)}\right| \\ &\lesssim |T|^{1/2}|v|_{1,T} + h_2^2|T|^{-1/2}(\|\partial_2 u_1\|_{0,T} + h_1|\partial_2 u_1|_{1,T}) \\ &\lesssim |T|^{1/2}(|u|_{1,T} + h_1|u|_{2,T}) \end{aligned}$$

where we have used again a local interpolation error estimate as we did in (5.2).

In treating the remaining term we cannot use the Poincaré inequality, instead we proceed as in the derivation of (5.5) and get by using (5.6) and (5.7)

$$\begin{aligned} \left|\int_{e_i} v\cdot n^{(i)}\right| &\le \int_{e_i} |v_1| + |v_2| \le |e_i|^{3/2}(\|\nabla v_1\cdot t^{(i)}\|_{0,e_i} + \|\nabla v_2\cdot t^{(i)}\|_{0,e_i}) \\ &\le |e_i|^{3/2}\left(\|\nabla u_1\cdot t^{(i)}\|_{0,e_i} + \|\nabla u_2\cdot t^{(i)}\|_{0,e_i}\right)\| \le |e_i|^{3/2}|u|_{1,e_i} \\ &\lesssim h_1^2|T|^{-1/2}(|u|_{1,T} + h_1|u|_{2,T}) \end{aligned} \tag{5.10}$$

where $t^{(i)}$ is the unit tangential vector at the edge e_i. Altogether we have derived

$$\begin{aligned}|A| &\lesssim |T|^{1/2}(|u|_{1,T} + h_1|u|_{2,T}) + h_1^{-1}h_2\, h_1^2|T|^{-1/2}(|u|_{1,T} + h_1|u|_{2,T}) \\ &\sim |T|^{1/2}(|u|_{1,T} + h_1|u|_{2,T}),\end{aligned}$$

and, analogously to (4.12),

$$\|\partial_2(d_2\,\lambda_3\lambda_1\,n^{(2)} + d_3\,\lambda_1\lambda_2\,n^{(3)})\| \lesssim |u|_{1,T} + h_1|u|_{2,T} \tag{5.11}$$

The remaining estimate is again obtained as in Subsection 4.2 but using this time (5.10):

$$\begin{aligned}\|\partial_1(d_2\,\lambda_3\lambda_1\,n^{(2)} + d_3\,\lambda_1\lambda_2\,n^{(3)})\| &\lesssim h_1^{-1}\|d_2\,\lambda_3\lambda_1\,n^{(2)} + d_3\,\lambda_1\lambda_2\,n^{(3)}\| \\ &\lesssim h_1^{-1}|T|^{1/2}(|d_2| + |d_3|) \\ &\lesssim h_1^{-1}|T|^{1/2}\,h_1^{-1}\left(\left|\int_{e_2} v\cdot n^{(2)}\right| + \left|\int_{e_3} v\cdot n^{(3)}\right|\right) \\ &\lesssim |u|_{1,T} + h_1|u|_{2,T}. \end{aligned}\tag{5.12}$$

With (5.2), (5.3), (5.9), (5.11), and (5.12) we have proved (3.12).

5.3 Trapezoidal elements

In the case of boundary layer patches there is nothing to prove since $X_H|_Q \subset X_h|_Q$, and therefore $\mathrm{I}_T v_H = v_H$ in T. In more general cases, however, it is not that simple. We will use the notation from Subsection 4.3, Figure 4.3, and proceed in analogy to Subsection 5.2.

Introducing the standard nodal interpolant N_T with respect to the vertices of T, we have the estimates (5.1) and (5.2):

$$\mathrm{I}_T u = \mathrm{N}_T u + (\mathrm{I}_T u - \mathrm{N}_T u) \tag{5.13}$$

$$|\mathrm{N}_T u|_{1,T} \lesssim |u|_{1,T} + h_1|u|_{2,T}, \tag{5.14}$$

and in analogy to (5.3)

$$\mathrm{I}_T u - \mathrm{N}_T u = \sum_{i=1}^{4} d_i b_i(x_1,x_2) n^{(i)}.$$

The coefficients d_i, $i = 1,\ldots,4$, are defined (using again $v := u - \mathrm{N}_T u$) as in (5.4) and can be estimated as in Subsection 5.2:

$$\begin{aligned}|d_i| &\sim |e_i|^{-1}\left|\int_{e_i} v\cdot n^{(i)}\right| \le |e_i|^{-1}\int_{e_i}(|v_1| + |v_2|) \\ &\le |e_i|^{-1}\int_{e_i}\left(\int_{e_i}|\nabla v_1\cdot t^{(i)}| + \int_{e_i}|\nabla v_2\cdot t^{(i)}|\right) \\ &\lesssim |e_i|^{1/2}\left(\|\nabla v_1\cdot t^{(i)}\|_{0,e_i} + \|\nabla v_2\cdot t^{(i)}\|_{0,e_i}\right) \\ &\lesssim |e_i|^{1/2}|u|_{1,e_i} \\ &\lesssim |e_i|\,|T|^{-1/2}(|u|_{1,T} + h_1|u|_{2,T}). \end{aligned}\tag{5.15}$$

The contributions from the short edges to $\mathrm{I}_T u - \mathrm{N}_T u$ can be estimated as in (5.9): For $i = 1, 3$, we obtain

$$|d_i b_i n^{(i)}|_{1,T} \lesssim |d_i| h_2^{-1} \|b_i\|_{0,T} \lesssim |u|_{1,T} + h_1 |u|_{2,T}. \tag{5.16}$$

The contributions from the long edges are treated similarly to Subsection 4.3, estimates (4.15)–(4.19):

$$d_4 b_4(x_1, x_2) \begin{bmatrix} 0 \\ 1 \end{bmatrix} + d_2 b_2(x_1, x_2) \begin{bmatrix} 0 \\ -1 \end{bmatrix} =: \begin{bmatrix} 0 \\ w \end{bmatrix}, \tag{5.17}$$

$$\begin{aligned} |w|_{1,T} &\lesssim h_1^{-1} \|\hat{\partial}_1 \hat{w}\|_{0,\hat{T}} + h_2^{-1} \|\hat{\partial}_2 \hat{w}\|_{0,\hat{T}} \\ &\sim h_1^{-1} |T|^{1/2} (|d_2| + |d_4|) + h_2^{-1} |T|^{1/2} |d_2 + d_4|, \\ |d_2 + d_4| &\lesssim h_2 |T|^{-1/2} |v_2|_{1,T} \lesssim h_2 |T|^{-1/2} h_1 |u_2|_{2,T}, \end{aligned}$$

such that with (5.15)

$$|w|_{1,T} \lesssim |u|_{1,T} + h_1 |u|_{2,T}. \tag{5.18}$$

Combining (5.13)–(5.18) we find the estimate that was to be shown.

Acknowledgement Both the visit of the first author in Valenciennes and the visit of the second author in Chemnitz were financed by the DFG (German Research Foundation), Sonderforschungsbereich 393.

References

[1] G. Acosta and R. G. Durán. The maximum angle condition for mixed and non-conforming elements. Application to the Stokes equations. *SIAM J. Numer. Anal.*, 37:18–36, 1999.

[2] M. Ainsworth and P. Coggins. The stability of mixed *hp*-finite element methods for Stokes flow on high aspect ratio elements. *SIAM J. Numer. Anal.*, 38:1721–1761, 2000.

[3] Th. Apel. *Anisotropic finite elements: Local estimates and applications.* Advances in Numerical Mathematics. Teubner, Stuttgart, 1999.

[4] Th. Apel, S. Nicaise, and J. Schöberl. A non-conforming finite element method with anisotropic mesh grading for the Stokes problem in domains with edges. *IMA J. Numer. Anal.*, 21:843–856, 2001.

[5] Th. Apel and H. M. Randrianarivony. Stability of discretizations of the Stokes problem on anisotropic meshes. *Mathematics and Computers in Simulation*, 61:437–447, 2003.

[6] R. Becker. *An adaptive finite element method for the incompressible Navier–Stokes equations on time-dependent domains.* PhD thesis, Ruprecht-Karls-Universität Heidelberg, 1995.

[7] R. Becker and R. Rannacher. Finite element solution of the incompressible Navier-Stokes equations on anisotropically refined meshes. In *Fast solvers for flow problems*, volume 49 of *Notes on Numerical Fluid Mechanics*, pages 52–62, Wiesbaden, 1995. Vieweg.

[8] C. Bernardi and G. Raugel. Analysis of some finite elements for the Stokes problem. *Math. Comp.*, 44:71–79, 1985.

[9] F. Brezzi and M. Fortin. *Mixed and hybrid finite element methods.* Springer, New York, 1991.

[10] P. G. Ciarlet. *The finite element method for elliptic problems.* North-Holland, Amsterdam, 1978.

[11] M. Fortin. Old and new finite elements for incompressible flows. *Int. J. Numer. Methods Fluids*, 1:347–354, 1981.

[12] V. Girault and P.-A. Raviart. *Finite element methods for Navier-Stokes equations, Theory and algorithms*, volume 5 of *Springer Series in Computational Mathematics.* Springer, Berlin, 1986.

[13] M. Randrianarivony. Stability of mixed finite element methods with anisotropic meshes. Master's thesis, TU Chemnitz, 2001.

[14] D. Schötzau and Ch. Schwab. Mixed *hp*-FEM on anisotropic meshes. *Math. Models Methods Appl. Sci.*, 8:787–820, 1998.

[15] D. Schötzau, Ch. Schwab, and R. Stenberg. Mixed *hp*-FEM on anisotropic meshes II: Hanging nodes and tensor products of boundary layer meshes. *Numer. Math.*, 83:667–697, 1999.

[16] J. L. Synge. *The hypercircle in mathematical physics.* Cambridge University Press, Cambridge, 1957.

[17] A. Toselli and C. Schwab. Mixed *hp*-finite element approximations on geometric edge and boundary layer meshes in three dimensions. SAM Report 2001-02, ETH Zürich, 2001.

Other titles in the SFB393 series:

02-01 M. Pester. Bibliotheken zur Entwicklung paralleler Algorithmen - Basisroutinen für Kommunikation und Grafik. Januar 2002.

02-02 M. Pester. Visualization Tools for 2D and 3D Finite Element Programs - User's Manual. January 2002.

02-03 H. Harbrecht, M. Konik, R. Schneider. Fully Discrete Wavelet Galerkin Schemes. January 2002.

02-04 G. Kunert. A posteriori error estimation for convection dominated problems on anisotropic meshes. March 2002.

02-05 H. Harbrecht, R. Schneider. Wavelet Galerkin Schemes for 3D-BEM. February 2002.

02-06 W. Dahmen, H. Harbrecht, R. Schneider. Compression Techniques for Boundary Integral Equations - Optimal Complexity Estimates. April 2002.

02-07 S. Grosman. Robust local problem error estimation for a singularly perturbed reaction-diffusion problem on anisotropic finite element meshes. May 2002.

02-08 M. Springmann, M. Kuna. Identifikation schädigungsmechanischer Materialparameter mit Hilfe nichtlinearer Optimierungsverfahren am Beispiel des Rousselier Modells. Mai 2002.

02-09 S. Beuchler, R. Schneider, C. Schwab. Multiresolution weighted norm equivalences and applications. July 2002.

02-10 Ph. Cain, R. A. Römer, M. E. Raikh. Renormalization group approach to energy level statistics at the integer quantum Hall transition. July 2002.

02-11 A. Eilmes, R. A. Römer, M. Schreiber. Localization properties of two interacting particles in a quasiperiodic potential with a metal-insulator transition. July 2002.

02-12 M. L. Ndawana, R. A. Römer, M. Schreiber. Scaling of the Level Compressibility at the Anderson Metal-Insulator Transition. September 2002.

02-13 Ph. Cain, R. A. Römer, M. E. Raikh. Real-space renormalization group approach to the quantum Hall transition. September 2002.

02-14 A. Jellal, E. H. Saidi, H. B. Geyer, R. A. Römer. A Matrix Model for $\nu_{k_1 k_2} = \frac{k_1+k_2}{k_1 k_2}$ Fractional Quantum Hall States. September 2002.

02-15 M. Randrianarivony, G. Brunnett. Parallel implementation of curve reconstruction from noisy samples. August 2002.

02-16 M. Randrianarivony, G. Brunnett. Parallel implementation of surface reconstruction from noisy samples. September 2002.

02-17 M. Morgenstern, J. Klijn, Chr. Meyer, R. A. Römer, R. Wiesendanger. Comparing measured and calculated local density of states in a disordered two-dimensional electron system. September 2002.

02-18 J. Hippold, G. Rünger. Task Pool Teams for Implementing Irregular Algorithms on Clusters of SMPs. October 2002.

02-19 H. Harbrecht, R. Schneider. Wavelets for the fast solution of boundary integral equations. October 2002.

02-20 H. Harbrecht, R. Schneider. Adaptive Wavelet Galerkin BEM. October 2002.

02-21 H. Harbrecht, R. Schneider. Wavelet Galerkin Schemes for Boundary Integral Equations - Implementation and Quadrature. October 2002.

03-01 E. Creusé, G. Kunert, S. Nicaise. A posteriory error estimation for the Stokes problem: Anisotropic and isotropic discretizations. January 2003.

03-02 S. I. Solov'ëv. Existence of the guided modes of an optical fiber. January 2003.

03-03 S. Beuchler. Wavelet preconditioners for the p-version of the FEM. February 2003.

03-04 S. Beuchler. Fast solvers for degenerated problems. February 2003.

03-05 A. Meyer. Stable calculation of the Jacobians for curved triangles. February 2003.

03-06 S. I. Solov'ëv. Eigenvibrations of a plate with elastically attached load. February 2003.

03-07 H. Harbrecht, R. Schneider. Wavelet based fast solution of boundary integral equations. February 2003.

03-08 S. I. Solov'ëv. Preconditioned iterative methods for monotone nonlinear eigenvalue problems. March 2003.

03-09 Th. Apel, N. Düvelmeyer. Transformation of hexahedral finite element meshes into tetrahedral meshes according to quality criteria. May 2003.

03-10 H. Harbrecht, R. Schneider. Biorthogonal wavelet bases for the boundary element method. April 2003.

03-11 T. Zhanlav. Some choices of moments of refinable function and applications. June 2003.

03-12 S. Beuchler. A Dirichlet-Dirichlet DD-pre-conditioner for p-FEM. June 2003.

03-13 Th. Apel, C. Pester. Clément-type interpolation on spherical domains - interpolation error estimates and application to a posteriori error estimation. July 2003.

03-14 S. Beuchler. Multi-level solver for degenerated problems with applications to p-version of the fem. *(Dissertation)* July 2003.

The complete list of current and former preprints is available via
`http://www.tu-chemnitz.de/sfb393/preprints.html`.